Highly Effective Separation of Semiconducting Carbon Nanotubes verified *via* Short-Channel Devices Fabricated Using Dip-Pen Nanolithography

Steve Park,[†] Hang Woo Lee,[‡] Huiliang Wang,[†] Selvapraba Selvarasah,[§] Mehmet R. Dokmeci,[§] Young Jun Park,[⊥] Seung Nam Cha,[⊥] Jong Min Kim,[⊥,*] and Zhenan Bao[‡,*]

[†]Department of Materials Science & Engineering and [‡]Department of Chemical Engineering, Stanford University, Stanford, California 94305, United States, [§]Department of Electrical & Computer Engineering, Northeastern University, Boston, Massachusetts 02115, United States, and [⊥]Frontier Research Lab, Samsung Advanced Institute of Technology, Korea

ABSTRACT We have verified a highly effective separation of semiconducting single-walled carbon nanotubes (sc-SWNTs) *via* statistical analysis of short-channel devices fabricated using multipen dip-pen nanolithography.

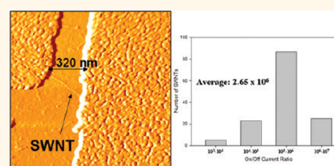

Our SWNT separation technique utilizes a polymer (rr-P3DDT) that selectively interacts with and disperses sc-SWNTs. Our devices had channel lengths on the order of 300−500 nm, with an average of about 3 SWNTs that directly connected the source−drain electrodes. A total of 140 SWNTs were characterized, through which we have observed that all of the SWNTs exhibited semiconducting behavior with an average on/off current ratio of $\sim 10^6$. Additionally, we have characterized 50 SWNTs after the removal of rr-P3DDT, through which we have again observed semiconducting behavior for all of the SWNTs with similar electrical characteristics. The relatively low average on-conductance of 0.0796 μS was attributed to the distribution of small diameter SWNTs in our system and due to the non-ohmic Au contacts on SWNTs. The largely positive threshold voltages were shifted toward zero after vacuum annealing, indicating that the SWNTs were doped in air. To the best of our knowledge, this is the first time numerous SWNTs were electrically characterized using short-channel devices, through which *all* of the measured SWNTs were determined to be semiconducting. Hence, our semiconducting single-walled carbon nanotube sorting system holds a great deal of promise in bringing forth a variety of practical applications in SWNT electronics.

KEYWORDS: carbon nanotubes · dip-pen nanolithography · sorting · nanofabrication · field-effect transistors · semiconducting · polythiophene

Since the first demonstration of single-walled carbon nanotube (SWNT) field-effect transistors (FETs) approximately a decade ago,[1,2] SWNTs have continuously attracted much attention in the research community due to their exceptional electrical properties, such as ballistic transport,[3−5] high charge carrier mobility,[6] and high compatibility to high-κ dielectric materials,[7−9] rendering them excellent candidates as building blocks for future nanoelectronic devices. Despite such an immense potential, the challenge of separating semiconducting SWNTs (sc-SWNTs) from metallic SWNTs (m-SWNTs) from an as-synthesized mixture in *high yields* has been the main drawback in the further advancement of carbon nanotube electronics. The presence of m-SWNTs, even under a small fraction, can drastically increase the off current, which is detrimental with respect to power consumption and transistor performance.[10] Therefore, finding an effective, low-cost, and a scalable method to separate out sc-SWNTs has been the focus of intense research over the past decade. In this respect, many research groups have developed techniques to selectively sort out sc-SWNTs, such as density gradient ultracentrifugation (DGU),[11] dielectrophoresis,[12−14] DNA-assisted separation,[15−18] selective chemical interactions,[19−21] and polymer-assisted separation.[22,23] For these techniques, the degree of SWNT separation was typically validated by optical absorption, photoluminescence excitation/emission (PLE) spectroscopy, and resonant Raman spectroscopy. However, such spectroscopic techniques do not provide the number of sc-SWNTs with respect to m-SWNTs in absolute quantities. To concretely validate the efficacy of sorting and to understand how the separation process affects the charge transport properties of the SWNTs, it is necessary to fabricate and characterize devices consisting of one to several SWNTs that directly bridge the source/drain (S/D) electrodes. Although some of the aforementioned separation techniques conducted thin-film SWNT-FET measurements, where channels on the order of

* Address correspondence to zbao@stanford.edu, jongkim@samsung.com.

Received for review December 13, 2011 and accepted February 20, 2012.

Published online February 21, 2012
10.1021/nn204875a

© 2012 American Chemical Society

tens of micrometers were composed of a percolating network of SWNTs, the absolute quantities of sc-SWNTs with respect to m-SWNTs and the electrical properties of the individual SWNTs still remained elusive. To address such an issue, Kim *et al.*[24] and Zhang *et al.*[25,26] have correlated spectroscopic data to the statistical counting of SWNTs by fabricating and measuring devices with channel lengths on the order of several hundred nanometers, where the S/D electrodes were bridged directly by individual SWNTs. These studies revealed that certain separation techniques still contained a significant amount of m-SWNTs, while other techniques exhibited devices with relatively low on/off ratios. Such results demonstrated that m-SWNTs had not yet been fully removed in these systems, while further validating the insufficiency of spectroscopic analysis in quantitatively determining sorting efficiency.

Recently, our group developed a method to separate out semiconducting HiPCO SWNTs from an as-synthesized mixture of commercially available HiPCO SWNTs utilizing regioregular poly(3-dodecylthiophene) (rr-P3DDT) that selectively interacts with and disperses sc-SWNTs.[27] Spectroscopic characterization techniques such as optical absorption, PLE spectra, and resonant Raman spectroscopy were conducted, through which we have speculated an efficient separation of sc-SWNTs.

For the present report, we have generated SWNT devices with a channel length in the range of 300–500 nm using dip-pen nanolithography[28−32] (DPN) to quantify the number of sc-SWNTs to m-SWNTs in our system and to characterize the electrical properties of the separated sc-SWNTs. We have characterized a total of 190 randomly sampled SWNTs prepared from multiple solutions and substrates and have observed that all of the SWNTs that we have measured were sc-SWNTs with an average on/off current ratio of $\sim 10^6$. As far as we know, this is the first time numerous SWNTs were electrically characterized using short-channel devices, through which *all* of the measured SWNTs were determined to be semiconducting. We have hence unambiguously validated the high sorting efficiency of our system that is both scalable and relatively facile to process. As mentioned previously, our results have great implications in future nanoelectronics, as even a small amount of m-SWNTs can dramatically increase the off current and degrade the transistor performance. In this report, we will first introduce our electrode fabrication process using DPN, originally developed by our group,[33,34] and present some advantages DPN has over the conventionally used e-beam lithography process (EBL). Second, we will present various experimental results validating the highly efficient sorting of sc-SWNTs. Lastly, we will discuss the electrical characteristics of our devices and present suggestions for future improvements.

RESULTS AND DISCUSSION

SWNT Device Fabrication Using Dip-Pen Nanolithography. To characterize the SWNTs in our system, we have fabricated short-channel SWNT-FETs using multipen dip-pen nanolithography[28−32] (DPN). Briefly stated, DPN is a process where an atomic force microscopy (AFM) tip is used to directly deposit a material of interest onto a surface with a high registration and precise feature size controllability.[35,36] Despite having similar resolution limits, we have selected DPN over the conventionally used e-beam lithography (EBL) process to generate contacts to the SWNTs due to a number of advantages DPN has over EBL. First, DPN requires relatively simple and fewer number of processing steps compared to EBL. Second, contrary to EBL, the DPN fabrication process does not expose the substrate to e-beam irradiation, which has previously been shown to damage the SWNTs.[37−39] Third, due to the use of a multipen array system, numerous electrodes can be fabricated in parallel in a time-efficient manner with shorter cycle time. Finally, since the throughput of DPN can easily be increased by increasing the number of tips on the chip, it can easily translate to large-area patterning applications.

Figure 1 depicts our experimental procedure of generating the SWNT-FETs using DPN. First, a solution of SWNT/rr-P3DDT in toluene was dispersed onto an APTMS-coated SiO_2 surface *via* spin-casting (APTMS: 3-aminopropyltrimethoxysilane). A heavily doped silicon substrate with a 300 nm thermally grown silicon oxide layer was used as the back gate and dielectric layer, respectively. The density of the SWNTs on the surface was controlled by the number of drops of solution cast on the substrate during spin-casting (refer to Supporting Information Figure S1 for results on SWNT density control test). Next, a thin film of Au ($\sim$15 nm) was evaporated onto the substrate, followed by an evaporation of additional Au ($\sim$50 nm) on top of the thin layer of Au using parylene shadow masks[40] to generate microscale pads for electrical probing.

Figure 2A is an optical image of the substrate after the two successive Au evaporations. The light red areas are the thin layered Au regions, whereas the bright yellow areas are the thicker Au regions that were generated using parylene shadow masks. Next, finer electrode features were generated by depositing an etch-resist known as 16-mercaptohexadecanoic acid (MHA) in a parallel manner between the microscale pads using DPN's multipen array system.[29,41] Finally, 15 nm of gold was etched away using wet-chemical etching,[42] leaving behind the microscale Au pads along with the Au underneath the etch-resist. Figure 2C is an optical image of an array of SWNT devices, and Figure 2B is an AFM phase image of one of the SWNT devices, while the inset is the corresponding topography image of the SWNT device. The DPN-generated

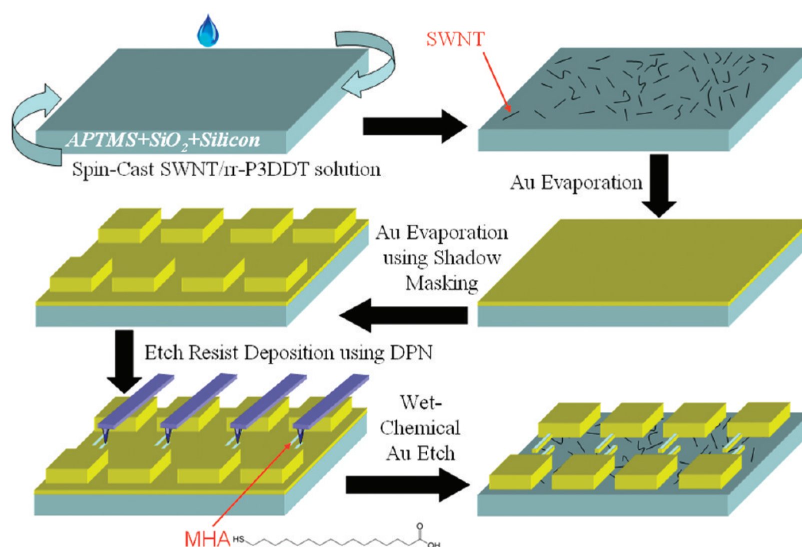

Figure 1. Schematic outline of SWNT device fabrication using dip-pen nanolithography. First, a SWNT/rr-P3DDT solution is spin-cast onto an APTMS-coated SiO_2/silicon substrate. Second, a thin layer of Au (15 nm) is evaporated, followed by an evaporation of additional Au (50 nm) using shadow masking. Next, an etch-resist (MHA) is deposited in a parallel manner using DPN's multipen array system. Finally, wet-chemical Au etching is conducted to etch away 15 nm of Au, leaving behind the Au underneath the etch-resist and the thicker Au regions.

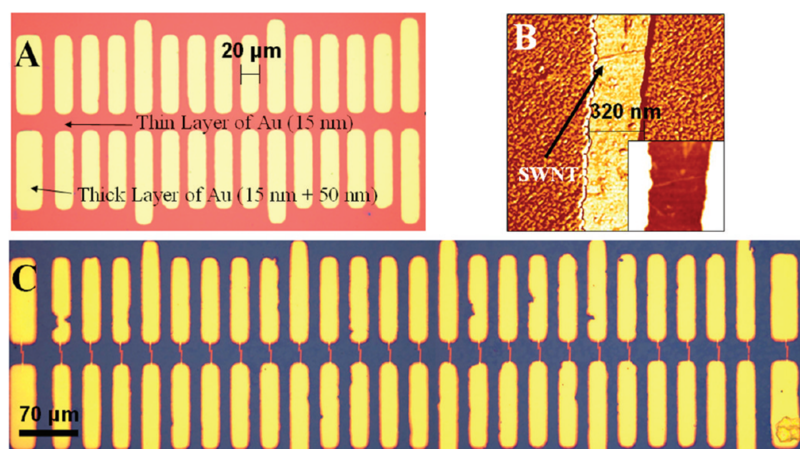

Figure 2. (A) Optical image of Au evaporated surface. The light red areas are the thin Au layer regions (thickness = 15 nm), and the bright yellow areas are the thicker Au layer regions that were generated using parylene shadow masking (thickness = 15 + 50 nm). (B) AFM phase image of a SWNT device; the inset is the corresponding topography image near the SWNT that is bridging the two electrode ends. (C) Optical image of an array of electrodes after parallel DPN etch-resist patterning and wet-chemical Au etching.

electrodes were generally etched cleanly with a low number of defects. Details regarding defect minimization and feature size controllability of our process are reported elsewhere.[34] The removal of Au on the SWNTs after Au etching was verified using X-ray photoemission spectroscopy (refer to Supporting Information Figure S2). The DPN-fabricated electrodes were controlled to have channel lengths in the range of 300–500 nm, enabling a few to several SWNTs to be bridged directly between the S/D electrodes. Further details of our fabrication process are reported in the Methods section.

Statistical Analysis of Sorting Efficiency. The SWNTs were prepared from two different solutions, and the devices were fabricated and measured on multiple substrates. The devices had an average of 3.3 SWNTs that directly connected the S/D electrodes, which summed to a total of 140 SWNTs. The SWNT/electrode contacts were verified by examining various AFM imaging modes (*i.e.*, topography, phase, error). Figure 3A,B shows the AFM phase and error images of two different SWNT devices that had two and one SWNTs that contacted the S/D electrodes, respectively. The insets within the images are the corresponding topography images, through which we have determined the heights of the SWNTs to be between 1 and 1.3 nm. We have estimated the on and off currents of individual SWNTs in our system by setting them equal to the on and off currents of the device divided by the total number of SWNTs on the device (*i.e.*, $I_{ON\text{-}SWNT} = I_{ON\text{-}DEVICE}/N$

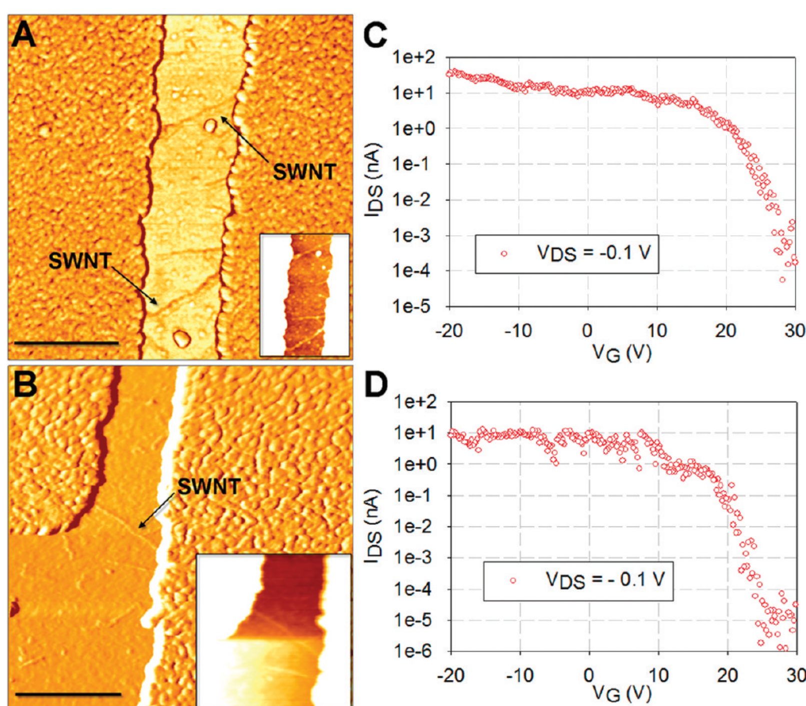

Figure 3. (A) AFM phase and (B) error images of two different SWNT devices. The scales bars are 500 nm. The insets within the images are the corresponding topography images. (C,D) Transfer curves of the devices shown in (A) and (B), respectively. The curves were swept from V_G = 30 V to −20 V at V_{DS} = −0.1 V. Both devices exhibited semiconducting behavior, with on/off current ratios between 10^5 and 10^6 and off currents in the range of 10^{-14} to 10^{-13} A.

and $I_{OFF\text{-}SWNT} = I_{OFF\text{-}DEVICE}/N$, where N is the total number of SWNTs connecting the source–drain electrodes).

The on and off currents of the devices were obtained using transfer curves, which were measured in the linear region from V_G = 30 to −20 V at V_{DS} = −0.1 V. Figure 3C,D shows the corresponding transfer curves of the devices shown in Figure 3A,B, respectively. The devices were measured under ambient conditions. Both devices evidently exhibited semiconducting behaviors with on/off current ratios between 10^5 and 10^6 and off currents in the range of 10^{-14} to 10^{-13} A. After measuring the rest of the devices, we have observed that all of the devices exhibited semiconducting behavior. Supporting Information Figure S3A–O shows AFM images and corresponding transfer curves of some of the other SWNT devices that were characterized. Figure 4A–C displays the histograms of the on current, off current, and the on/off current ratio of the 140 SWNTs with average values of 7.96 × 10^{-9} A, 1.77 × 10^{-14} A, and 2.65 × 10^6, respectively. Field-effect mobility of the SWNTs was not calculated due to the dominant contact resistance of the devices, rendering it difficult to extract the intrinsic mobility of SWNTs (this topic will be discussed in the next section). As Figure 4B,C indicates, the range of on/off current ratio and off current of the SWNTs were 10^3–10^7 and 10^{-16}–10^{-12} A, respectively. The low off currents of the SWNTs and the on/off current ratios being no less than 10^3 indicated that all 140 SWNTs were semiconducting, as any m-SWNTs that directly bridged the S/D electrodes would have exhibited a large off current and short the device.

To confirm that the observed high on/off ratio is not due to any potential interaction between the rr-P3DDT residue and the SWNTs, we investigated the electrical properties of the SWNTs after the removal of rr-P3DDT. After spin-casting a solution of SWNT/rr-P3DDT onto a substrate, we heated the substrate at 500 °C under argon for 1 h to burn away rr-P3DDT while preserving the SWNTs (HiPCO SWNTs have been determined to be stable up to ~800 °C).[43]

Figure 5A,B shows resonant Raman spectra before and after heating, respectively. Evidently, the rr-P3DDT peaks at ~1379 and ~1445 cm^{-1} are no longer present after heating, indicating that rr-P3DDT has been removed from the substrates. Considering also the AFM topography images before and after heating in Figure 5C,D, respectively, the average diameters of SWNTs have been reduced from ~1.2 to ~0.9 nm, further supporting the conclusion of removal of rr-P3DDT after heating. Electrodes were fabricated onto the polymer-burned SWNT substrates, and a total of 50 SWNTs were characterized using the aforementioned analytical approach. Again, all 50 SWNTs showed semiconducting behavior, with an average on current, off current, and on/off current ratio of 4.46 × 10^{-9} A, 2.1 × 10^{-14} A, and 1.55 × 10^6, respectively (refer to Supporting Information Figure S4 for corresponding histograms).

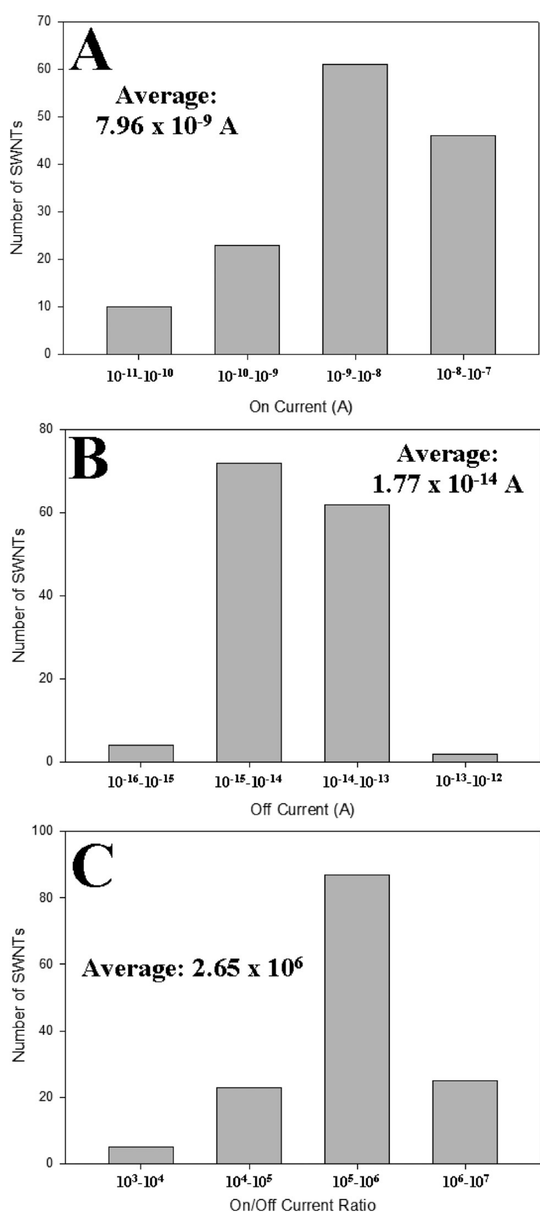

Figure 4. Histogram of (A) on current, (B) off current, and (C) on/off current ratios of individual SWNTs based on 140 SWNTs, measured at V_{DS} = −0.1 V.

These values were quite similar to the previously attained values for SWNT devices with rr-P3DDT. Supporting Information Figure S3P−T is the AFM images and corresponding transfer curves of some of the polymer-burned SWNT devices that were characterized. Again, the on/off current ratios of the SWNTs were no less than 10^3, with off currents in the range of 10^{-15} to 10^{-12} A. Two main conclusions can be drawn from our results. The fact that no metallic behavior was observed even after burning off rr-P3DDT and that the electronic properties of the polymer-burned SWNTs were similar to the polymer-present SWNTs (1) removes the possibility of m-SWNTs exhibiting semiconducting behavior due to the presence of rr-P3DDT and (2) that the SWNTs are the dominant charge carriers in our devices.

In order to verify the presence of m-SWNTs originally in the as-synthesized HiPCO SWNTs that we have used in our study, using the same fabrication process, we have generated electrodes on as-synthesized HiPCO SWNTs (refer to the Methods section for experimental procedure). Out of 10 devices that we have measured, four devices exhibited semiconducting behavior with on/off current ratios between 10^4 and 10^7. Three of the devices exhibited semimetallic behavior with on/off current ratios of ∼10 and off currents ranging from 10^{-9} to 10^{-8} A; the other three devices showed metallic behavior with no current modulation at 10^{-8} to 10^{-7} A. Supporting Information Figure S5 shows AFM images and corresponding transfer curves of two of the as-synthesized SWNT devices that were characterized. These results verified the presence of m-SWNTs originally in the as-synthesized HiPCO SWNTs that we have used in our study, and that our sorting technique did indeed effectively separate out sc-SWNTs from m-SWNTs.

Analysis of Contact Resistance and the Observed On-Conductance. Previous reports have proposed that short-channel SWNT devices operate as Schottky barrier (SB) transistors.[2,44−49] In SB transistors, current through the channel is limited by the barrier at the SWNT/metal interface, and the applied gate and drain−source bias modulates the barrier width, hence the tunneling current through the barrier.[44,50] Since the tunneling current can be modulated by source−drain voltage, the output curve of SB transistors is diotic in nature, where the current continuously increases beyond a certain source−drain voltage even when the device is in the off-state.[1] The output curves of our devices exhibited diotic behavior, indicating that our devices operate as SB transistors.

Figure 6A,B displays the output curve and the AFM image of a SWNT device, respectively. The device had two SWNTs that directly contacted the S/D electrodes. The inset within Figure 6A is the corresponding transfer curve that clearly exhibits semiconducting characteristics at V_{DS} = −0.1 V, with an off current of $\sim 10^{-13}$ A. However, referring to the output curve where V_{DS} was swept from 0 to −5 V with gate bias modulated from 30 to −5 V in steps of 5 V, the current undergoes a large increase at $V_{DS} < -1$ even when the device is in the off-state at V_G = 30 V, a clear indication of a typical diotic behavior of a SB transistor.

One of the consequences of SB transistors is the limited on-conductance due to the Schottky barrier at the SWNT/metal interface. As mentioned previously, the average on current of our SWNTs was 7.96×10^{-9} A at V_{DS} = −0.1 V, which gives an average on-conductance of 0.0796 μS. One of the reasons for the relatively low on-conductance of our SWNT devices can be attributed to the distribution of small diameter SWNTs in

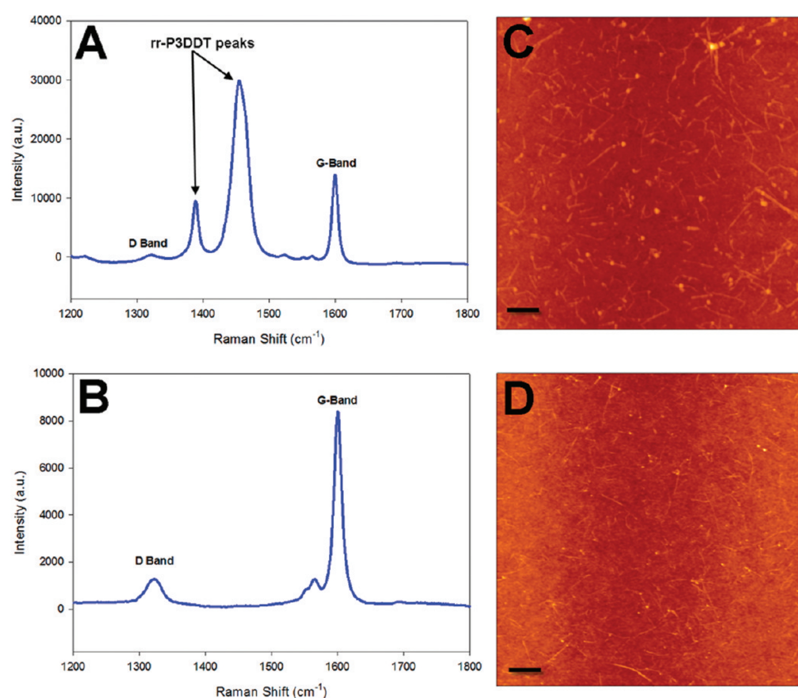

Figure 5. Representative resonant Raman spectroscopy of SWNT substrates (A) before and (B) after burning off rr-P3DDT. AFM topography images of SWNT substrates (C) before and (D) after burning of rr-P3DDT. The scale bars are 500 nm.

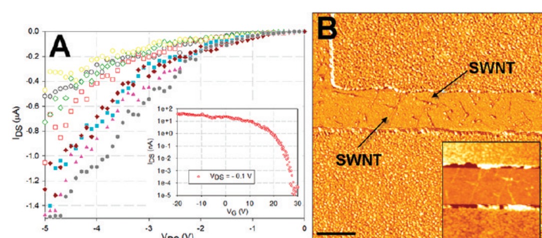

Figure 6. (A) Output curve of the SWNT device swept from V_{DS} of 0 to −5 V with V_G modulated from 30 to −5 V in steps of 5 V. The inset is the corresponding transfer curve with V_{DS} = −0.1 V. (B) AFM image of the device showing two SWNTs directly contacting the S/D electrodes. The scale bar is 500 nm.

our system. On the basis of PLE data in our previous work,[27] a SWNT of (12,1) chirality is the most dominant SWNT type in our system, which has a diameter of 0.995 nm.[27] Previous works have demonstrated that SWNTs with smaller diameters exhibited lower on currents due to a larger Schottky barrier,[47,49] where the I_{ON} of 1 nm diameter SWNTs was approximately an order of magnitude lower than I_{ON} of 1.5 nm diameter SWNTs.[49] The on-conductance obtained by other groups[2,44,45] on SWNTs with diameters of ∼1.4 to 1.6 nm is indeed approximately an order of magnitude higher than the average on-conductance of our devices. Hence, considering that the dominant SWNTs in our system were 0.995 nm in diameter, our on-conductance values are within a reasonable range.

Apart from contact resistance arising from Schottky barrier, a pure tunneling barrier may also exist due to poor interaction between the SWNT and the metal contacts, which can consequently lower the on-conductance. Both *ab initio*[51] and experimental[52] studies have confirmed that Au interacts poorly with SWNTs in comparison to other metals. Such a weak interaction may result in a large vacuum formation at the interface, preventing efficient injection of carriers.[47] For this reason, other contact metals such as Pd have been used by other groups, which demonstrated high device performance.[5,9] Efforts are currently underway to improve the on-conductance of our devices by investigating other contact metals.

Analysis of Threshold Voltage. The threshold voltages of our devices were between ∼25 and 30 V when swept from V_G = 30 to −20 V in air. Such a positively shifted threshold voltage can be attributed to the p-type doping of SWNTs. Since the SWNTs are solution processed under ultrasonication, defects are likely to form along the SWNT surface, which can act as oxidation sites for O_2 and H_2O in air.[53] According to works by Derycke *et al.*,[45] the degree of doping of SWNTs was related to the degree of change in the threshold voltage. Figure 7 is the transfer characteristics of a SWNT device measured in air and under N_2 after vacuum annealing at 80 °C for 10 min, where V_G was swept from 50 to −50 V at V_{DS} = −0.1 V.

The shift in the threshold voltage to the left from ∼40 to ∼5 V after vacuum annealing indicates that the SWNT was indeed doped in air, and that vacuum annealing had desorbed the O_2 and/or H_2O on the SWNTs. In addition, the decrease in the on current after vacuum annealing is consistent with previous results[45,46] and can be explained by the increase in

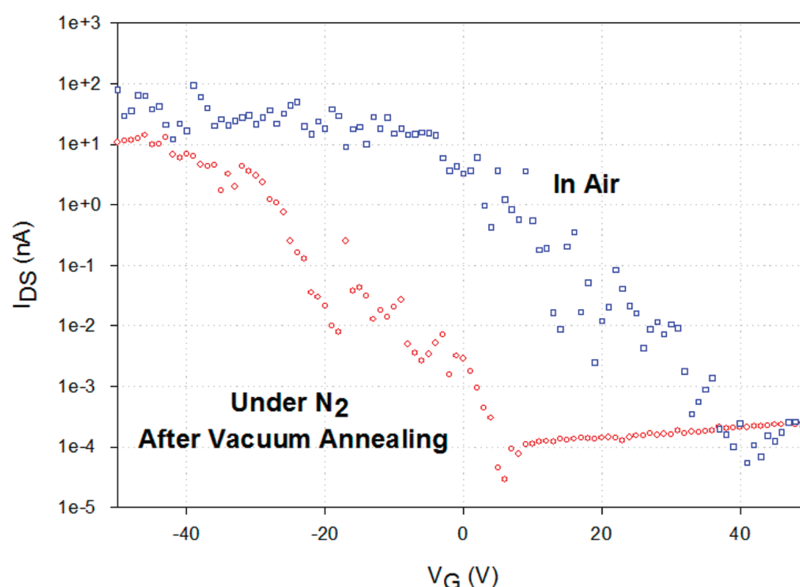

Figure 7. Transfer characteristics of a SWNT device measured in air and in a nitrogen glovebox after vacuum annealing at 80 °C for 10 min. V_G was swept from 50 to −50 V at V_{DS} = −0.1 V.

the Schottky barrier due to the rise in the Fermi level of the metal and due to the shifting of the SWNT Fermi level toward the middle of the band gap. Interestingly, Derycke *et al.*[45] observed no shift in the threshold voltage upon vacuum annealing and exposing the SWNT device to O_2, through which they have concluded that their SWNTs were not doped by O_2. On the contrary, we speculate that our SWNTs were doped from defects formed during solution processing followed by the exposure to excessive O_2 and H_2O during the fabrication process (*i.e.*, wet-chemical etching). Investigation is currently being conducted to further understand the origin and the nature of threshold voltage and doping in our devices.

CONCLUSIONS

Herein, we have verified a highly effective separation of sc-SWNTs using statistical analysis of short-channel devices that were fabricated *via* multipen dip-pen nanolithography. We have measured a total of 140 SWNTs and have verified that all of the SWNTs were semiconducting with an average on/off current ratio of $\sim 10^6$. Furthermore, upon measuring 50 additional SWNTs after burning off rr-P3DDT, we have confirmed once again that all 50 SWNTs were semiconducting with similar electrical properties. The relatively low on-conductance of our devices was attributed to the distribution of small diameter SWNTs in our system and the non-ohmic contacts of Au on SWNTs. By annealing and measuring the devices under N_2, the threshold voltages shifted toward zero, indicating that our SWNTs were doped by O_2 and/or H_2O during our fabrication process. We expect that, with further research, such as improving and understanding device performance and developing a reliable method to generate a densely aligned array of SWNTs in a controllable manner, a number of practical applications will soon be realized.

METHODS

Substrate Cleaning and Preparation. A heavily doped silicon substrate with 300 nm thermally grown oxide layer was diced into 1 × 2 cm pieces, immersed in piranha solution (1:3 ratio of hydrogen peroxide/sulfuric acid) for 30 min, rinsed in running DI water for 10 min, and dried in a vacuum oven for 15 min at 80 °C. The substrates were then taken into a nitrogen glovebox and immersed into a 0.4 vol % solution of APTMS (3-aminopropyltrimethoxysilane) in anhydrous toluene for 1 h. This step generated a monolayer of APTMS on the SiO_2 surface and was conducted inside a nitrogen glovebox to prevent the active polymerization of APTMS in the presence of water in the atmosphere. APTMS surfaces were generated to enhance the adhesion of SWNTs[54] and the evaporated Au.[34] The substrates were then taken out of the glovebox, rinsed several times with toluene, and ultrasonicated in toluene for 10 min to remove excess APTMS on the surface. Finally, the substrates were dried with a N_2 air gun and placed in a vacuum oven for 15 min at 80 °C. These APTMS-coated substrates were used for all of the experiments in this study.

SWNT Solution Preparation. To prepare the selectively dispersed solution of sc-SWNTs wrapped with rr-P3DDT, 5 mg of HiPCO SWNTs purchased from Unidym Inc. and 5 mg of regioregular poly(3-dodecylthiophene) (rr-P3DDT) purchased from Sigma Aldrich Inc. were mixed into 25 mL of toluene. Toluene, which has low solubility to SWNTs, was used to ensure that only polymer-wrapped SWNTs were dispersed in the solution, while the unwrapped SWNTs can eventually be separated out. The solution was sonicated using an ultrasonicator (Cole Parmer Ultrasonic Processor 750 W) at an amplitude level of 70% for 30 min at 50 °C using a temperature-controlled cooling bath system. The temperature control system was implemented because the efficiency of polymer wrapping around SWNTs is dependent on the temperature during sonication.[27] Next, the solution was centrifuged for 150 min at 42 000*g* to collapse the

nondispersed SWNTs and other insoluble materials to the bottom of the centrifuge tube. Finally, the supernatant was carefully extracted and placed into a separate vial.

We have also made a solution of as-synthesized HiPCO SWNTs by adding 5 mg of HiPCO SWNTs in 25 mL of NMP (*N*-methyl-2-pyrrolidone, EMD) and sonicating the solution for 10 min at an amplitude level of 30%. The solution vial was kept in ice water during sonication to prevent the over heating of the solution due to sonication. NMP was used instead of toluene due to the low solubility of SWNTs in toluene in the absence of a dispersant. The purpose of making this solution was to test the presence of m-SWNTs in the as-synthesized sample of HiPCO SWNTs that were used in our study.

Spin-Casting and Au Evaporation. The APTMS-coated substrates were spun at 4000 rpm, and two 10 μL drops of the SWNT/rr-P3DDT solution were cast on each of the substrates with an interval of 10 s between the two drops. This step generated a dense yet nonpercolating network of SWNTs on the substrate. In addition, also at 4000 rpm, five 10 μL drops of the as-synthesized HiPCO solution were cast on another set of substrates, also at an interval of 10 s between the drops. Lastly, all of the substrates were heated in a vacuum oven at 80 °C for 10 min to remove any remaining solvent on the substrates. To remove rr-P3DDT on some of the substrates, we heated the substrate to 500 °C for 1 h under argon flow at 790 Torr.

Next, 15 nm of Au was thermally evaporated uniformly onto all of the substrates at an evaporation rate of 0.5 Å/s. Subsequently, parylene shadow masks[40] were placed on top of the substrates, and 50 nm of additional Au was thermally evaporated also at an evaporation rate of 0.5 Å/s. This step generated thicker regions of microscale Au pads that would eventually be used as pads for electrical probing. As depicted in Figure 2, the parylene mask had 2 $\times$ 26 (row by column) arrays of rectangles with dimensions of 100 μm $\times$ 20 μm (length $\times$ width); the lateral and vertical edge-to-edge spacing between the rectangles were 15 and 20 μm, respectively. The rectangles on the right most and the left most ends of the array had dimensions of 100 μm $\times$ 30 μm in length and width, respectively. These rectangular arrays were designed to match the tip-to-tip spacing of the multipen array used in our experiments.

DPN and Au Wet-Chemical Etching. A 26 pen cantilever array (Type F-Side F1), obtained from NanoInk Inc., was placed in an UV ozone cleaner for 10 min. Next, the cantilever array was immersed in a 5 mM solution of 16-mercaptohexadecanoic acid (MHA) in acetonitrile for 10 s, dried gently with N_2 air gun, and reimmersed in the MHA solution for another 10 s. Subsequently, the MHA-coated cantilever array was mounted on the NSCRIPTOR DPN system (purchased from NanoInk Inc.), and MHA was deposited onto a Au-coated substrate in a parallel manner to form a stable self-assembled monolayer that would later function as an etch mask. The MHA was patterned in the shape of electrodes between the microscale Au pads with electrode gaps ranging from 300 to 500 nm. The deposition rate and hence the feature sizes of the patterned MHA were controlled by using the ink calibration feature in the InkCAD software. Further details regarding the DPN electrode fabrication process can be found in a previously reported work.[34]

$Fe(NO_3)_3$/thiourea solution[42] was used for Au wet-chemical etching prepared *via* a 1:1 mixture of 26.6 mM $Fe(NO_3)_3 \cdot 9(H_2O)$ (J.T. Baker) and 40 mM thiourea (Alfa Aesar) in octanol-saturated H_2O. This solution was adjusted to pH 2 by the addition of HCl (10 μL of HCl for a 5 mL $Fe(NO_3)_3$/thiourea solution). The MHA-patterned substrate was immersed in the Au etchant for 6 min under constant stirring at 100 rpm to etch away 15 nm of Au (etching rate is approximately 2.5 nm/min), leaving behind the protected Au underneath the MHA along with the thicker Au pad regions that were previously generated using parylene shadow masking. Next, the substrate was rinsed in DI water, gently dried with N_2 gas, and examined under a microscope for visual inspection. If the Au etch was observed to be incomplete, the substrate was immersed back into the etchant for 30 s and re-examined under the microscope; this step was repeated until the Au appeared to be sufficiently etched. Such a meticulous procedure was taken due to the possibility of overetching the Au that degrades the quality of the DPN-patterned electrodes.

Characterization of the SWNTs and SWNT Devices. The resonant Raman scattering (RRS, model LabRam Aramis from Horiba Jobin Yvon) was carried out at 1.96 eV (633 nm) excitation at 100$\times$ magnification and 1 μm spot size, and 1200 grating. Excitation power was 5 mW. The peak positions were calibrated with the Si line at 521 cm^{-1}.

Electrical measurements on the SWNT transistors were conducted using a Keithley 4200 SC semiconductor analyzer both in air and inside a nitrogen glovebox. The heavily doped silicon substrate was used as the back gate. The SWNTs between the S/D electrodes were imaged using ACT-50 tapping mode probes purchased from AppNano Inc. and the InkCAD software on the NSCRIPTOR DPN system. The AFM images were processed using NanoRule (Pacific Nanotechnology).

Conflict of Interest: The authors declare no competing financial interest.

Acknowledgment. We thank S. Morishita for providing the SWNT/rr-P3DDT solution for this project. We also thank O. Johnson for conducting XPS. We thank the National Science Foundation (ECCS 0901414 and Award No. 1059020) for funding.

Supporting Information Available: AFM images showing SWNT density control using different number of SWNT drops cast during spin-coating (Figure S1). XPS data showing the removal of Au after wet-chemical etching (Figure S2). AFM images and their corresponding transfer curves of various SWNT devices before and after polymer burning (Figure S3). Histogram of on current, off current, and on/off current ratio of SWNT devices after polymer burnoff (Figure S4). AFM images and their corresponding transfer curves of unsorted SWNT devices (Figure S5). This material is available free of charge *via* the Internet at http://pubs.acs.org.

REFERENCES AND NOTES

1. Tans, S. J.; Verschueren, A. R. M.; Dekker, C. Room-Temperature Transistor Based on a Single Carbon Nanotube. *Nature* **1998**, *393*, 49–52.
2. Martel, R.; Schmidt, T.; Shea, H. R.; Hertel, T.; Avouris, P. Single- and Multi-Wall Carbon Nanotube Field-Effect Transistors. *Appl. Phys. Lett.* **1998**, *73*, 2447–2449.
3. Wind, S. J.; Appenzeller, J.; Avouris, P. Lateral Scaling in Carbon-Nanotube Field-Effect Transistors. *Phys. Rev. Lett.* **2003**, *91*, 4.
4. Javey, A.; Guo, J.; Paulsson, M.; Wang, Q.; Mann, D.; Lundstrom, M.; Dai, H. J. High-Field Quasiballistic Transport in Short Carbon Nanotubes. *Phys. Rev. Lett.* **2004**, *92*, 4.
5. Javey, A.; Guo, J.; Wang, Q.; Lundstrom, M.; Dai, H. J. Ballistic Carbon Nanotube Field-Effect Transistors. *Nature* **2003**, *424*, 654–657.
6. Durkop, T.; Getty, S. A.; Cobas, E.; Fuhrer, M. S. Extraordinary Mobility in Semiconducting Carbon Nanotubes. *Nano Lett.* **2004**, *4*, 35–39.
7. Javey, A.; Tu, R.; Farmer, D. B.; Guo, J.; Gordon, R. G.; Dai, H. J. High Performance n-Type Carbon Nanotube Field-Effect Transistors with Chemically Doped Contacts. *Nano Lett.* **2005**, *5*, 345–348.
8. Javey, A.; Kim, H.; Brink, M.; Wang, Q.; Ural, A.; Guo, J.; McIntyre, P.; McEuen, P.; Lundstrom, M.; Dai, H. J. High-κ Dielectrics for Advanced Carbon-Nanotube Transistors and Logic Gates. *Nat. Mater.* **2002**, *1*, 241–246.
9. Javey, A.; Guo, J.; Farmer, D. B.; Wang, Q.; Wang, D. W.; Gordon, R. G.; Lundstrom, M.; Dai, H. J. Carbon Nanotube Field-Effect Transistors with Integrated Ohmic Contacts and High-κ Gate Dielectrics. *Nano Lett.* **2004**, *4*, 447–450.
10. Sarker, B. K.; Shekhar, S.; Khondaker, S. I. Semiconducting Enriched Carbon Nanotube Aligned Arrays of Tunable Density and Their Electrical Transport Properties. *ACS Nano* **2011**, *5*, 6297–6305.
11. Arnold, M. S.; Green, A. A.; Hulvat, J. F.; Stupp, S. I.; Hersam, M. C. Sorting Carbon Nanotubes by Electronic Structure Using Density Differentiation. *Nat. Nanotechnol.* **2006**, *1*, 60–65.
12. Krupke, R.; Hennrich, F.; Kappes, M. M.; Lohneysen, H. V. Surface Conductance Induced Dielectrophoresis of Semiconducting

Single-Walled Carbon Nanotubes. *Nano Lett.* **2004**, *4*, 1395–1399.
13. Krupke, R.; Hennrich, F.; von Lohneysen, H.; Kappes, M. M. Separation of Metallic from Semiconducting Single-Walled Carbon Nanotubes. *Science* **2003**, *301*, 344–347.
14. Peng, H. Q.; Alvarez, N. T.; Kittrell, C.; Hauge, R. H.; Schmidt, H. K. Dielectrophoresis Field Flow Fractionation of Single-Walled Carbon Nanotubes. *J. Am. Chem. Soc.* **2006**, *128*, 8396–8397.
15. Ming, Z.; Jagota, A.; Semke, E. D.; Diner, B. A.; McLean, R. S.; Lustig, S. R.; Richardson, R. E.; Tassi, N. G. DNA-Assisted Dispersion and Separation of Carbon Nanotubes. *Nat. Mater.* **2003**, *2*, 338–342.
16. Zheng, M.; Jagota, A.; Strano, M. S.; Santos, A. P.; Barone, P.; Chou, S. G.; Diner, B. A.; Dresselhaus, M. S.; McLean, R. S.; Onoa, G. B.; *et al.* Structure-Based Carbon Nanotube Sorting by Sequence-Dependent DNA Assembly. *Science* **2003**, *302*, 1545–1548.
17. Zheng, M.; Semke, E. D. Enrichment of Single Chirality Carbon Nanotubes. *J. Am. Chem. Soc.* **2007**, *129*, 6084–6085.
18. Tu, X. M.; Manohar, S.; Jagota, A.; Zheng, M. DNA Sequence Motifs for Structure-Specific Recognition and Separation of Carbon Nanotubes. *Nature* **2009**, *460*, 250–253.
19. Strano, M. S.; Dyke, C. A.; Usrey, M. L.; Barone, P. W.; Allen, M. J.; Shan, H. W.; Kittrell, C.; Hauge, R. H.; Tour, J. M.; Smalley, R. E. Electronic Structure Control of Single-Walled Carbon Nanotube Functionalization. *Science* **2003**, *301*, 1519–1522.
20. Li, H. P.; Zhou, B.; Lin, Y.; Gu, L. R.; Wang, W.; Fernando, K. A. S.; Kumar, S.; Allard, L. F.; Sun, Y. P. Selective Interactions of Porphyrins with Semiconducting Single-Walled Carbon Nanotubes. *J. Am. Chem. Soc.* **2004**, *126*, 1014–1015.
21. Yang, C. M.; An, K. H.; Park, J. S.; Park, K. A.; Lim, S. C.; Cho, S. H.; Lee, Y. S.; Park, W.; Park, C. Y.; Lee, Y. H. Preferential Etching of Metallic Single-Walled Carbon Nanotubes with Small Diameter by Fluorine Gas. *Phys. Rev. B* **2006**, *73*, 7.
22. Nish, A.; Hwang, J. Y.; Doig, J.; Nicholas, R. J. Highly Selective Dispersion of Single Walled Carbon Nanotubes Using Aromatic Polymers. *Nat. Nanotechnol.* **2007**, *2*, 640–646.
23. Yi, W. H.; Malkovskiy, A.; Chu, Q. H.; Sokolov, A. P.; Colon, M. L.; Meador, M.; Pang, Y. Wrapping of Single-Walled Carbon Nanotubes by a π-Conjugated Polymer: The Role of Polymer Conformation-Controlled Size Selectivity. *J. Phys. Chem. B* **2008**, *112*, 12263–12269.
24. Kim, W. J.; Lee, C. Y.; O'Brien, K. P.; Plombon, J. J.; Blackwell, J. M.; Strano, M. S. Connecting Single Molecule Electrical Measurements to Ensemble Spectroscopic Properties for Quantification of Single-Walled Carbon Nanotube Separation. *J. Am. Chem. Soc.* **2009**, *131*, 3128–3129.
25. Zhang, L.; Zaric, S.; Tu, X. M.; Wang, X. R.; Zhao, W.; Dai, H. J. Assessment of Chemically Separated Carbon Nanotubes for Nanoelectronics. *J. Am. Chem. Soc.* **2008**, *130*, 2686–2691.
26. Zhang, L.; Tu, X. M.; Welsher, K.; Wang, X. R.; Zheng, M.; Dai, H. J. Optical Characterizations and Electronic Devices of Nearly Pure (10,5) Single-Walled Carbon Nanotubes. *J. Am. Chem. Soc.* **2009**, *131*, 2454–2455.
27. Lee, H. W.; Yoon, Y.; Park, S.; Oh, J. H.; Hong, S.; Liyanage, L. S.; Wong, P. H. S.; Tok, J. B. H.; Kim, J. M.; Bao, Z.; *et al.* Selective Dispersion of High Purity Semiconducting Single-Walled Carbon Nanotubes with Regioregular Poly (3-alkylthiophene)s. *Nat. Commun.* **2011**, *2*, 541.
28. Hong, S. H.; Zhu, J.; Mirkin, C. A. Multiple Ink Nanolithography: Toward a Multiple-Pen Nano-Plotter. *Science* **1999**, *286*, 523–525.
29. Hong, S. H.; Mirkin, C. A. A Nanoplotter with Both Parallel and Serial Writing Capabilities. *Science* **2000**, *288*, 1808–1811.
30. Liu, X. G.; Zhang, Y.; Goswami, D. K.; Okasinski, J. S.; Salaita, K.; Sun, P.; Bedzyk, M. J.; Mirkin, C. A. The Controlled Evolution of a Polymer Single Crystal. *Science* **2005**, *307*, 1763–1766.
31. Piner, R. D.; Zhu, J.; Xu, F.; Hong, S. H.; Mirkin, C. A. "Dip-Pen" Nanolithography. *Science* **1999**, *283*, 661–663.
32. Haaheim, J.; Eby, R.; Nelson, M.; Fragala, J.; Rosner, B.; Zhang, H.; Athas, G. Dip Pen Nanolithography (DPN): Process and Instrument Performance with NanoInk's NSCRIPTOR System. *Ultramicroscopy* **2005**, *103*, 117–132.
33. Wang, W. M.; LeMieux, M. C.; Selvarasah, S.; Dokmeci, M. R.; Bao, Z. Dip-Pen Nanolithography of Electrical Contacts to Single-Walled Carbon Nanotubes. *ACS Nano* **2009**, *3*, 3543–3551.
34. Park, S.; Wang, W. M.; Bao, Z. Parallel Fabrication of Electrode Arrays on Single-Walled Carbon Nanotubes Using Dip-Pen-Nanolithography-Patterned Etch Masks. *Langmuir* **2009**, *26*, 6853–6859.
35. Weinberger, D. A.; Hong, S.; Mirkin, C. A.; Wessels, B. W.; Higgins, T. B. Combinatorial Generation and Analysis of Nanometer- and Micrometer-Scale Silicon Features *via* "Dip-Pen" Nanolithography and Wet Chemical Etching. *Adv. Mater.* **2000**, *12*, 1600–1603.
36. Zhang, H.; Chung, S.-W.; Mirkin, C. A. Fabrication of Sub-50-nm Solid-State Nanostructures on the Basis of Dip-Pen Nanolithography. *Nano Lett.* **2003**, *3*, 43–45.
37. Smith, B. W.; Luzzi, D. E. Electron Irradiation Effects in Single Wall Carbon Nanotubes. *J. Appl. Phys.* **2001**, *90*, 3509–3515.
38. Vijayaraghavan, A.; Kanzaki, K.; Suzuki, S.; Kobayashi, Y.; Inokawa, H.; Ono, Y.; Kar, S.; Ajayan, P. M. Metal-Semiconductor Transition in Single-Walled Carbon Nanotubes Induced by Low-Energy Electron Irradiation. *Nano Lett.* **2005**, *5*, 1575–1579.
39. Suzuki, S.; Kobayashi, Y. Diameter Dependence of Low-Energy Electron and Photon Irradiation Damage in Single-Walled Carbon Nanotubes. *Chem. Phys. Lett.* **2006**, *430*, 370–374.
40. Selvarasah, S.; Chao, S. H.; Chen, C. L.; Sridhar, S.; Busnaina, A.; Khademhosseini, A.; Dokmeci, M. R. A Reusable High Aspect Ratio Parylene-C Shadow Mask Technology for Diverse Micropatterning Applications. *Sens. Actuators, A* **2008**, *145*, 306–315.
41. Salaita, K.; Lee, S. W.; Wang, X. F.; Huang, L.; Dellinger, T. M.; Liu, C.; Mirkin, C. A. Sub-100 nm, Centimeter-Scale, Parallel Dip-Pen Nanolithography. *Small* **2005**, *1*, 940–945.
42. Geissler, M.; Wolf, H.; Stutz, R.; Delamarche, E.; Grummt, U. W.; Michel, B.; Bietsch, A. Fabrication of Metal Nanowires Using Microcontact Printing. *Langmuir* **2003**, *19*, 6301–6311.
43. Thostenson, E. T.; Li, C.; Chou, T.-W. Nanocomposites in Context. *Compos. Sci. Technol.* **2005**, *65*, 491–516.
44. Appenzeller, J.; Knoch, J.; Derycke, V.; Martel, R.; Wind, S.; Avouris, P. Field-Modulated Carrier Transport in Carbon Nanotube Transistors. *Phys. Rev. Lett.* **2002**, *89*, 126801.
45. Derycke, V.; Martel, R.; Appenzeller, J.; Avouris, P. Controlling Doping and Carrier Injection in Carbon Nanotube Transistors. *Appl. Phys. Lett.* **2002**, *80*, 2773–2775.
46. Heinze, S.; Tersoff, J.; Martel, R.; Derycke, V.; Appenzeller, J.; Avouris, P. Carbon Nanotubes as Schottky Barrier Transistors. *Phys. Rev. Lett.* **2002**, *89*, 106801.
47. Kim, W.; Javey, A.; Tu, R.; Cao, J.; Wang, Q.; Dai, H. J. Electrical Contacts to Carbon Nanotubes down to 1 nm in Diameter. *Appl. Phys. Lett.* **2005**, *87*, 3.
48. Nosho, Y.; Ohno, Y.; Kishimoto, S.; Mizutani, T. Relation between Conduction Property and Work Function of Contact Metal in Carbon Nanotube Field-Effect Transistors. *Nanotechnology* **2006**, *17*, 3412–3415.
49. Chen, Z. H.; Appenzeller, J.; Knoch, J.; Lin, Y. M.; Avouris, P. The Role of Metal-Nanotube Contact in the Performance of Carbon Nanotube Field-Effect Transistors. *Nano Lett.* **2005**, *5*, 1497–1502.
50. Zhou, C. W.; Kong, J.; Dai, H. J. Electrical Measurements of Individual Semiconducting Single-Walled Carbon Nanotubes of Various Diameters. *Appl. Phys. Lett.* **2000**, *76*, 1597–1599.
51. Shan, B.; Cho, K. J. *Ab Initio* Study of Schottky Barriers at Metal-Nanotube Contacts. *Phys. Rev. B* **2004**, *70*, 4.

52. Zhang, Y.; Franklin, N. W.; Chen, R. J.; Dai, H. J. Metal Coating on Suspended Carbon Nanotubes and Its Implication to Metal-Tube Interaction. *Chem. Phys. Lett.* **2000**, *331*, 35–41.
53. Collins, P. G.; Bradley, K.; Ishigami, M.; Zettl, A. Extreme Oxygen Sensitivity of Electronic Properties of Carbon Nanotubes. *Science* **2000**, *287*, 1801–1804.
54. Liu, J.; Casavant, M. J.; Cox, M.; Walters, D. A.; Boul, P.; Lu, W.; Rimberg, A. J.; Smith, K. A.; Colbert, D. T.; Smalley, R. E. Controlled Deposition of Individual Single-Walled Carbon Nanotubes on Chemically Functionalized Templates. *Chem. Phys. Lett.* **1999**, *303*, 125–129.